Phase-shift correction of seismic reflections by means of spectral recomposition

Zuniga, Nelson Ricardo Coelho Flores; Draganov, Deyan; Ghose, Ranajit

DOI
10.1002/nsg.12271

Publication date
2023

Document Version
Final published version

Published in
Near Surface Geophysics

Citation (APA)
Zuniga, N. R. C. F., Draganov, D., & Ghose, R. (2023). Phase-shift correction of seismic reflections by means of spectral recomposition. *Near Surface Geophysics*, *21*(6), 414-426. https://doi.org/10.1002/nsg.12271

Received: 21 November 2022 | Accepted: 25 August 2023

DOI: 10.1002/nsg.12271

Near Surface Geophysics EAGE EUROPEAN ASSOCIATION OF GEOSCIENTISTS & ENGINEERS

ORIGINAL ARTICLE

Phase-shift correction of seismic reflections by means of spectral recomposition

Nelson Ricardo Coelho Flores Zuniga[1] | **Deyan Draganov**[2] | **Ranajit Ghose**[2]

[1]Department of Mining and Petroleum Engineering, Escola Politécnica da Universidade de São Paulo (EP-USP), São Paulo, São Paulo, Brazil

[2]Faculty of Civil Engineering and Geosciences, Delft University of Technology, Delft, The Netherlands

Correspondence
Nelson Ricardo Coelho Flores Zuniga, Department of Mining and Petroleum Engineering, Escola Politécnica da Universidade de São Paulo (EP-USP), Cidade Universitária, São Paulo, SP, Brazil.
Email: nelson.zuniga@iag.usp.br

Funding information
Coordenação de Aperfeiçoamento de Pessoal de Nível Superior (CAPES); Conselho Nacional de Desenvolvimento Científico e Tecnológico (CNPq)

Abstract
Using post-critical reflection data, it is possible to obtain useful information that allows more reliable geological characterization of the subsurface. However, the strong distortion caused by the phase shift in post-critical wavelets makes the use of post-critical reflections rather challenging. For this reason, an approach which is capable of estimating the phase shift of each wavelet of a reflection event in a data-driven manner is desirable. In this vein, in case the frequency spectrum of a wavelet can be correctly estimated, it is possible to estimate the instantaneous phase shift. In this work, we propose an approach which can perform such estimation based on spectral recomposition of seismic data. We design an inversion approach in order to reconstruct the seismic spectrum of the wavelets of a reflection event, which subsequently allows us to estimate the instantaneous phase of each wavelet of the near-surface reflection events without performing prior velocity analysis and/or critical-angle estimation. After finding the instantaneous phase for each wavelet of a reflection event, we show next how one can find the respective phase shifts that can then be corrected.

KEYWORDS
frequency, inversion, phase, seismic, shallow subsurface

INTRODUCTION

Due to sharp changes in seismic velocity with depth in the shallow subsurface, in near-surface seismic reflection data, the critical angle (CA) is quickly reached at relatively short offsets, as compared to deeper, exploration-scale data. CAs at a subsurface boundary represent an important piece of information for seismic data analyses (e.g., Liu et al., 2011). However, post-critical reflections are usually used separately from the pre-critical ones, thus missing the benefit of a more complete utilization of seismic reflection information across the offsets. The position of the CA is highly relevant in common-mid-point (CMP) stacking, as obtaining a stacked image of high signal-to-noise ratio (SNR) demands disregarding post-critical information in order to minimize stacking of phase-shifted wavelets. As the wave phase rotates abruptly in the vicinity of the CA and because, in near-surface seismic imaging, the CA is reached quickly, the number of usable traces used to perform the stacking tends to be limited (Paskvish, 2016; Purves, 2014; Roth et al., 1998; Zelt et al., 2013). CA information is usually obtained from Snell's law (Roth et al., 1998; Zelt et al., 2013), which demands reliable prior estimation of the compressional (P) and/or shear (S) wave velocities. However, uncertainties in velocity estimates above and below an interface result in uncertainties in estimating the CAs. For this reason, an approach that is capable of estimating and correcting the phase shift in each wavelet in a reflection event without prior velocity and CA calculation is highly desirable. This will enable having more traces available for CMP stacking.

Spectral recomposition is a technique that can be used to extract the key components of a seismic spectrum (Cai et al., 2013; Li et al., 2011; Tomasso et al., 2010). It is usually performed by estimating the fundamental signal properties, such as peak frequency, amplitude and phase, in order to reconstruct the seismic spectrum (Cai et al., 2013; Castagna et al., 2003;

Tomasso et al., 2010). This allows reconstructing a seismic spectrum through an inversion procedure, if there is a mathematical description for the analysed wavelet available. In this way, the recovery of the peak frequency, amplitude and phase of a wavelet can be achieved.

We develop an inversion approach in order to reconstruct the spectrum of a seismic reflection event and then estimate its phase shift. Following Zuniga et al. (2023), at first we fit a calculated spectrum to the observed one, where the calculated spectrum is the mathematical representation of the Ricker wavelet (Ricker, 1953), and the observed spectrum represents the recorded reflection wavelet. This enables correcting the phase shifts such that the phase difference between the post-critical reflections and the reflection events at near offsets is greatly reduced, allowing the use of more traces and achieving a higher SNR in the stacking process.

The curve fitting is performed for each wavelet along a reflection event in a common-source gather. After recovering the peak frequency and the amplitude information from each wavelet, we use each peak frequency as the input information in order to fit the calculated phase to an observed one. The calculated phase is the exponential part in the mathematical representation of the Ricker wavelet, and the observed phase is the phase of the recorded reflection event. In this way, it is possible to estimate the phase shift of each trace and correct it to make it more alike the first recorded wavelet in an event.

Different from other methods for obtaining the phase shift (e.g., Barros et al., 2015; Biondi et al., 2014; Landro & Tsvankin, 2006; Zhu & McMechan, 2012), our approach allows obtaining wave parameters and phase-shift information in order to correct the phase shift of each wavelet in a reflection event in a data-driven manner and without the need of performing velocity analysis or prior CA estimation. Additionally, our approach requires shorter offsets when compared with other similar existing techniques (e.g., Landro & Tsvankin, 2006).

THEORY

Spectral recomposition

The spectrum of a seismic trace can be represented as a sum of different Ricker-wavelets spectra, as proposed by (Tomasso et al., 2010):

$$d(f) \approx \sum_{i=1}^{n} a_i \psi_i (m_i, f), \tag{1}$$

where, $d(f)$ is the spectrum of a seismic trace, f is frequency, and a_i and m_i are the amplitude and the peak frequency of the ith Ricker-wavelet spectrum, respectively. A Ricker-wavelet spectrum with a peak frequency at m is given by:

$$R(f) = a\psi(m, f) = a\frac{f^2}{m^2}\exp\left(-\frac{f^2}{m^2}\right). \tag{2}$$

Spectral recomposition can be used to obtain the peak frequency and amplitude from a seismic spectrum by reconstructing it, which differs from other approaches which instead decompose the seismic spectrum (Cai et al., 2013; Castagna et al., 2003; Huang et al., 1998; Li et al., 2011).

With the above mathematical description of the frequency spectrum, it is possible to handle the problem as an inversion which aims to fit, for each trace, a calculated frequency spectrum to the spectrum of an observed reflection wavelet. In this way, we can recover the peak frequency and the amplitude (Zuniga et al., 2023).

In Equation (2), $R(f)$ represents the observed wavelet, whereas the right-hand side of the equation represents the calculated wavelet.

Instantaneous-phase estimation

To estimate the instantaneous phase of this wavelet, another consideration is necessary. First, we need to calculate the argument of Equation (2), similar to the approach proposed by Zuniga et al. (2023) for estimating the position in time of a wavelet:

$$\arg\left[R(f)\right] = \arg\left[a\frac{f^2}{m^2}\exp\left(-\frac{f^2}{m^2}\right)\right]. \tag{3}$$

From Equation (3), we find that:

$$\arg\left[R(f)\right] = -\frac{f^2}{m^2}. \tag{4}$$

Considering n number of traces, we can rewrite Equation (4) as:

$$\arg\left[R_n(f)\right] = -\frac{f^2}{m_n^2}. \tag{5}$$

As each wavelet in a given reflection event presents a specific phase shift along the offset, we can describe the shift in phase for this event in the nth trace relative to the phase in the first ($n = 1$) trace. For the first trace, we get:

$$\arg\left[R_1(f)\right] = -\frac{f^2}{m_1^2} + \varphi_1 = -\frac{f^2}{m_1^2} + 0, \tag{6}$$

where φ is the instantaneous phase shift. In this case, $\varphi = \varphi_1$ is equal to zero.

For each $n > 1$, there is a different peak frequency (m) value. Therefore, the term $-f^2/m_n^2$ is different for different traces. φ_n represents how much the phase of the wavelet in the nth trace differs in comparison with that of the wavelet in the first trace for the same reflection event (i.e. instantaneous phase shift):

$$\arg\,[R_1\,(f)] = -\frac{f^2}{m_n^2} + \varphi_n\,. \tag{7}$$

In Equation (7), the term $\arg[R_1(f)]$ represents the observed instantaneous phase, whereas the right-hand side of the equation represents the calculated instantaneous phase.

Finding the instantaneous-phase shift for each wavelet allows us to correct each phase in each trace by rotating it until it gets close to the wavelet in the first trace. This enables us using the reflection information at offsets beyond the CA, which is otherwise not possible.

ALGORITHM

Finding the peak frequency

With the description given in Equation (2), it is possible to calculate the frequency spectrum of the Ricker wavelet. Once the wavelet of a reflection event in a trace (observed wavelet) is selected, it is then transformed to the frequency domain, where it is possible to fit the spectrum calculated using Equation (2) to the spectrum of the observed wavelet. We apply an inversion approach to perform the curve fitting (Zuniga et al., 2023). As the spectrum of the Ricker wavelet is an observed quantity, the parameters to be inverted for are the peak frequency m and the amplitude a.

To avoid falling in local minima in a global search, we use a multi-start procedure in a local optimization algorithm (Telraky & Sotirov, 2013). This combination allows performing several iterations with randomized starting points and provides a good statistical distribution of regions containing the minimum. We perform least-square minimization. In the stochastic process, each iteration results in a different minimum value, which can be compared to the minima from other iterations. Then, it is possible to select the lowest of all minima. The number of iterations can be set to adapt to the complexity of the analysed spectra, increasing the accuracy and efficiency of recovering the parameters related to the global minimum region.

The inversion procedure is applied to each trace for a selected reflection event, resulting in a set of peak frequencies and amplitudes. Additionally, the obtained optimum set of parameters (along with the associated uncertainties) for each trace is saved.

Finding the instantaneous-phase shift

Using Equation (7), it is possible to calculate the instantaneous phase of the Ricker-wavelet. The procedure is applied for the same selected event in each trace to estimate the peak-frequency m. The estimated peak-frequency values, corresponding to different traces, are used to calculate the instantaneous-phase shift φ (Equation 7), through fitting the calculated instantaneous phase to the observed one.

Similar to peak-frequency estimation, we next carry out an inversion to perform the curve fitting. As the instantaneous phase of the Ricker-wavelet is an observed quantity, the parameter to be inverted for is the instantaneous-phase shift φ. We employ the same procedure as that for peak-frequency estimation to avoid using a global-search algorithm.

The flow chart of the complete algorithm is presented in Figure 1.

RESULTS

Two-layered models

The new approach can obtain instantaneous phase shift without the requirement of prior velocity-analysis for CA estimation. This allows correction of any variation in the phase of a reflection wavelet in each trace along the measurement line.

We test our approach by analysing the reflection events from three simple near-surface S-wave models. Each model represents a two-layered subsurface with an interface located at 6 m depth. The lower layer has an S-wave velocity of 200 m/s, whereas the upper layer has an S-wave velocity of 100, 120 and 140 m/s, in the first, second and third models, respectively. We simulate an S-wave survey using a finite-difference modelling scheme (Thorbecke & Draganov, 2011). For our tests, we pick the primary reflection from the interface between the two layers. The first model presents a CA at 30.00° (Figure 2a), the second one at 36.87° (Figure 2b) and the third one at 44.43° (Figure 2c). Note, that the refraction visually separates from the post-critical reflection at an angle higher than the CA, giving the false impression that the CA is marked at a lower incidence angle.

In Figure 3, the original wavelet for several traces from the model shown in Figure 2a and their rotations as they approach the CA are shown. We also illustrate here each of the phases corrected through instantaneous-phase rotation estimated by our method. The same can be observed, in Figures 4 and 5, for the models presented in Figure 2b,c, respectively.

The above example is oversimplified as the arrivals are clear and they hardly suffer from interferences. In field data, there will be many more arrivals, and also

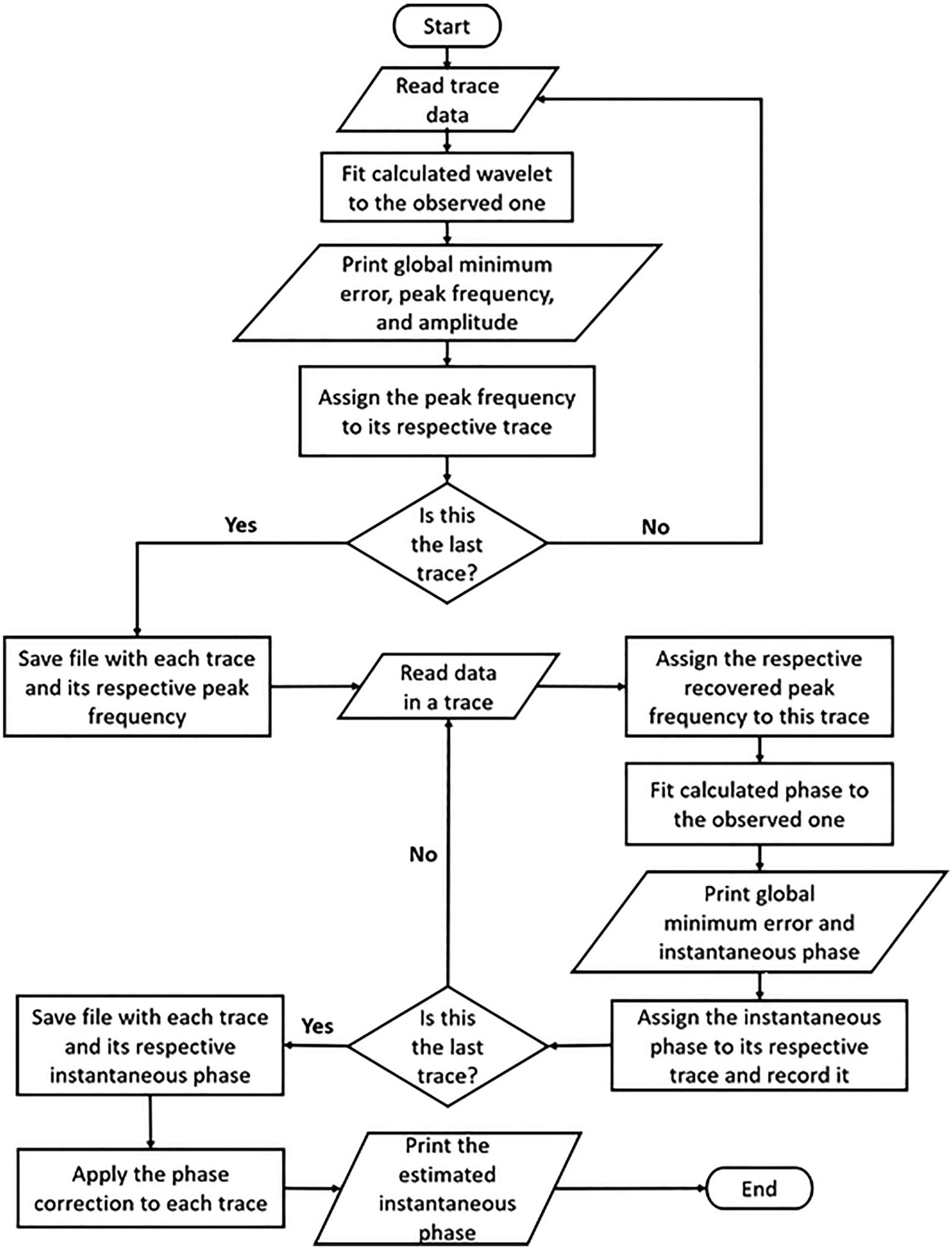

FIGURE 1 Flow chart of the proposed algorithm.

noise. To test the performance of our approach, we add Gaussian noise with SNR = 2 to the data of Figure 2 in order to obtain the events shown in Figure 6.

Figure 7 illustrates the variation of the instantaneous phase as a function of the incidence angle for the noisy (SNR = 2) data and its comparison with noise-free data. For the primary reflection event in Figure 6a, Figure 7a shows that a more abrupt increase in phase shift occurs when the incidence angle approaches the CA. Beyond the CA, the phase shift decreases gradually. The same observations are made in Figure 7b,c for the primary events in Figure 6b,c, respectively.

For the above-mentioned three models, obtaining the exact incidence angle or the trace associated with the CA is difficult, as the region with a phase shift around 180° is rather large. Nevertheless, the approach is

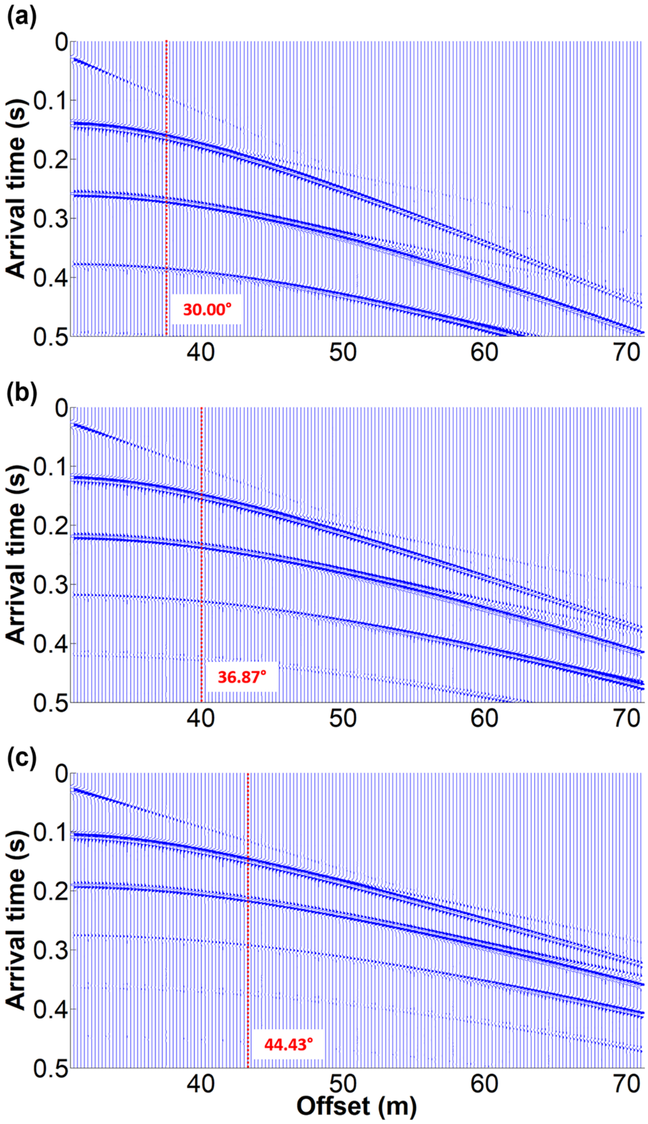

FIGURE 2 Simulated common-source gathers for the three two-layered models used in our tests. The primary reflection for the three models is characterized by a critical angle (CA) at (a) 30.00°, (b) 36.87° and (c) 44.43°, indicated by red dotted line.

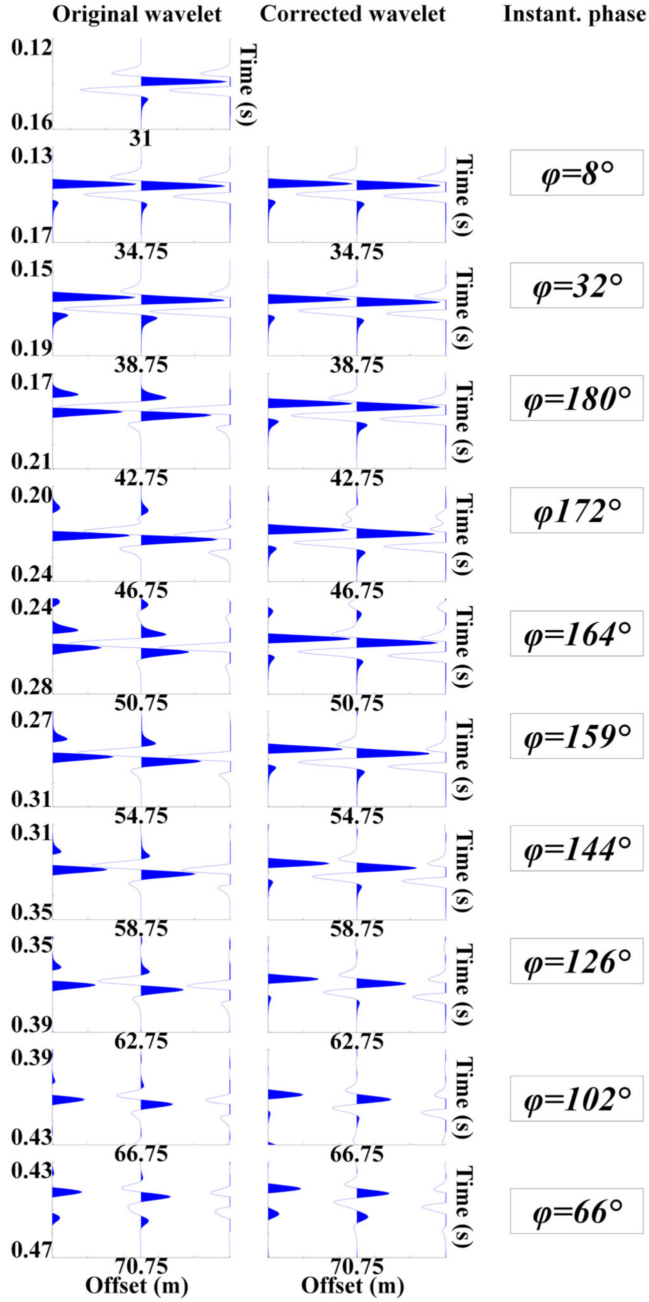

FIGURE 3 Original wavelets from the traces shown in Figure 2A (first column), the corrected wavelets (second column) and the phase shift in degree relative to the first recorded wavelet (third column) for the chosen reflection event.

quite effective in finding the phase shift/rotation in each wavelet, thus allowing for correction for such phase shift.

Comparing the detected behaviour of the instantaneous phase with angle for data without and with noise, we see that the examples with SNR = 2 show small errors in the estimates (Figure 8).

Figure 8a–c shows the normalized instantaneous-phase error between the estimates for data without noise and with noise as a function of the incidence angle of the primary reflection event. For each of them, the normalized error varies in a very similar manner, with a higher error at the near offsets (i.e. at lower incident angles) and a quick decrease of error at higher incidence angles. This allows us to perform a stable phase-shift correction, even for data with a significantly low SNR and for traces showing a larger phase shift.

Four-layered model inspired by field data

Encouraged by the test results from the above simple models, we test our approach further by analysing synthetic reflection events from a more realistic near-surface model. This model was inspired by the field data of Gibbs et al. (1992). The model represents a four-layered subsurface with two unsaturated layers located above two saturated layers, with the water table at 13 m depth. The parameters of the model are shown in Table 1. We

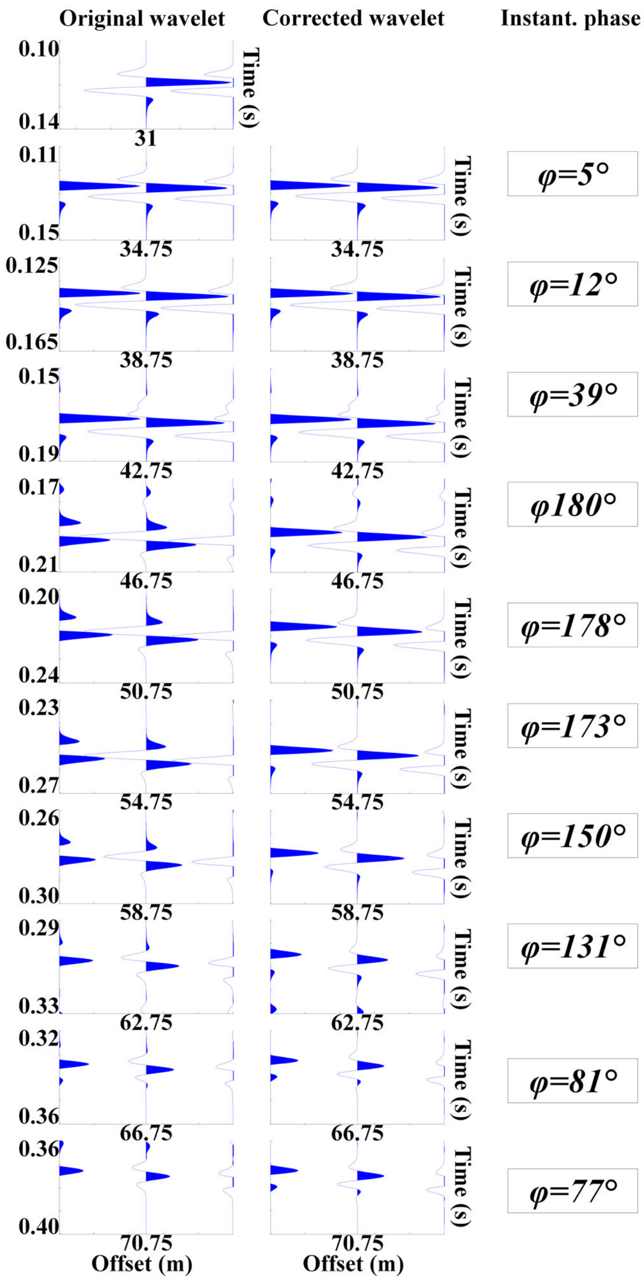

FIGURE 4 Same as in Figure 3, but for the traces shown in Figure 2b.

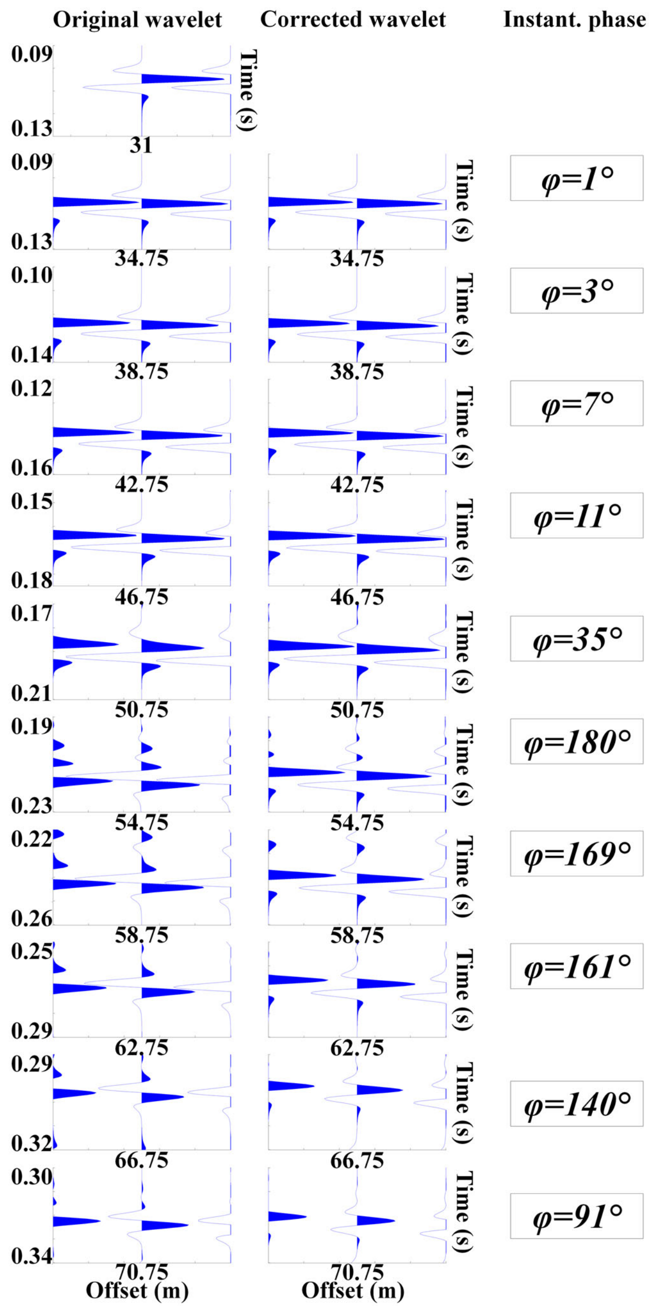

FIGURE 5 Same as in Figure 3, but for the traces shown in Figure 2c.

simulate a survey using P- and S-wave sources, in the same manner as in the previous example, except that this time the model does not include a free surface. This means that surface waves and free-surface multiples are not present. In the case of field data, surface-wave suppression has to be performed a priori, for example using a data-driven interferometric surface-wave suppression approach (Balestrini et al., 2020), followed by surface-related multiple suppression as successfully attempted in the past (e.g., Ghose & Goudswaard, 2004). Note that having the free-surface multiples in data is not a limitation for the application of this method. At traces where a free-surface multiple interferes with a target event, the estimation will work poorly as the wavelet will no more be simple. Nevertheless, where interference does not occur, the estimation will still work, which will result in an improved SNR of a stacked target reflection arrival as there will be also traces after the CA with corrected phase rotation.

The simulated common-source gather for this model, representing the wavefield recorded by a vertical-particle-velocity sensor due to a pressure source, is shown in Figure 9a. In Figure 9b, we see the same gather but after adding uncorrelated Gaussian noise (SNR = 2).

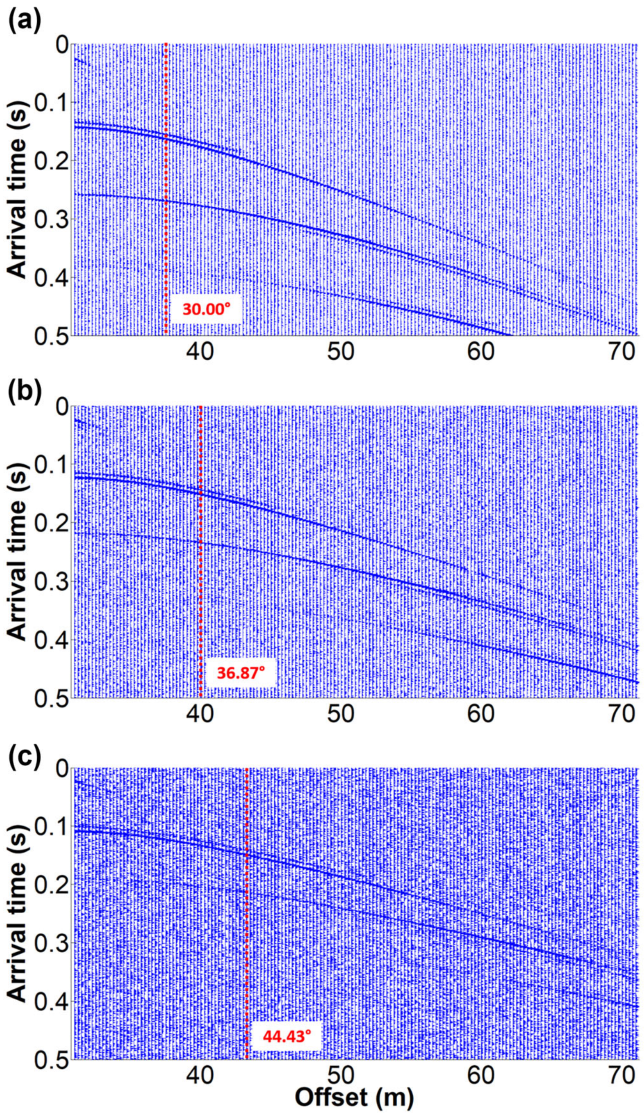

FIGURE 6 Simulated common-source gathers for the three two-layered models, with signal-to-noise ratio (SNR) = 2, used in our tests. The primary reflection for each gather is characterized by a critical angle (CA) at (a) 30.00°, (b) 36.87° and (c) 44.43°, indicated in red.

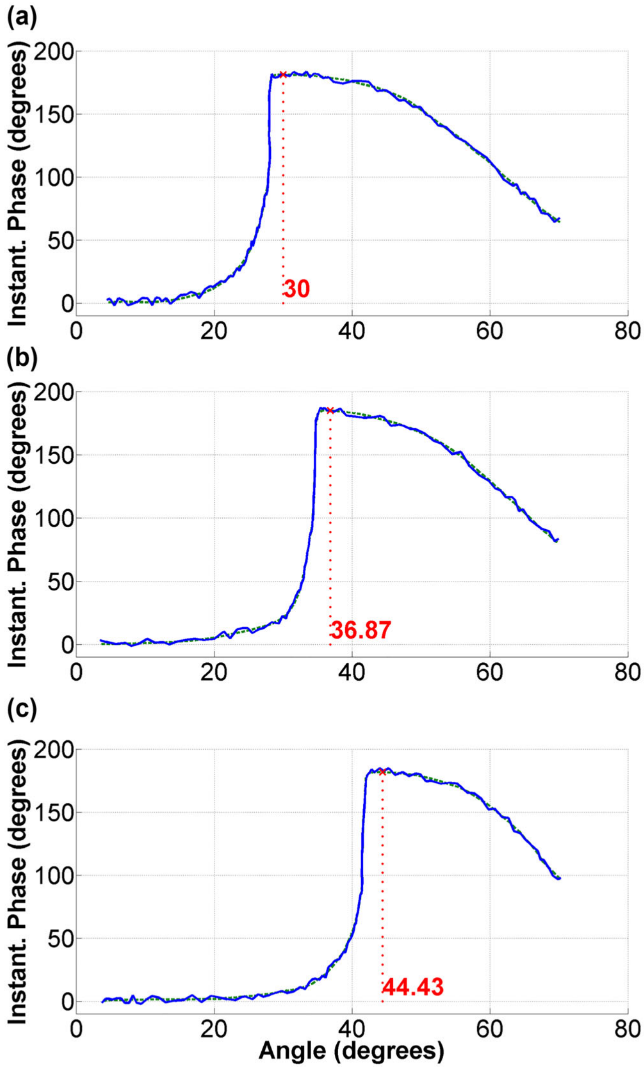

FIGURE 7 Variation of the instantaneous phase as a function of the incidence angle for noisy (signal-to-noise ratio [SNR] = 2, bold blue line) data for the primary reflection event corresponding to (a) Figure 6a, (b) Figure 6b and (c) Figure 6c. The correct critical angle (CA) value is indicated in red for comparison. Moreover, for comparison, the dashed green lines show the results for noise-free data.

We use both these gathers to estimate the CAs and the instantaneous-phase shift required to correct the rotation of wavelets of reflection events corresponding to the three interfaces in the shallow subsurface.

We can see in Figure 9 that, in case of a more complex, realistic situation, the approach suffers from the interference of events from different layer boundaries and of different wave types. In Figures 10–12, we illustrate for comparison the variation of the instantaneous phase with the incidence angle for noise-free and noisy (SNR = 2) data for PP, SS and SP events, respectively.

For the reflection event corresponding to the first interface shown in Figure 9, Figures 10a and 11a indicate a gentle increase in the phase shift as compared to the shift observed in Figure 12a. It can be explained by the fact that the CA of the SP reflection event is smaller than that of the PP and the SS reflection events. A gradual decrease beyond the CA can be observed for these three events too. The same observations can be made for the reflection event corresponding to the second interface, by comparing Figures 10b and 11b with Figure 12b. For the reflection event corresponding to the third interface, we observe again the same relation, as we compare Figures 10c and 11c with Figure 12c. However, Figures 10b, 11b and 12b show very different values for the CA when compared with other layers, which can be explained by the abrupt change in P-wave velocity that occurs between the second and the third layers.

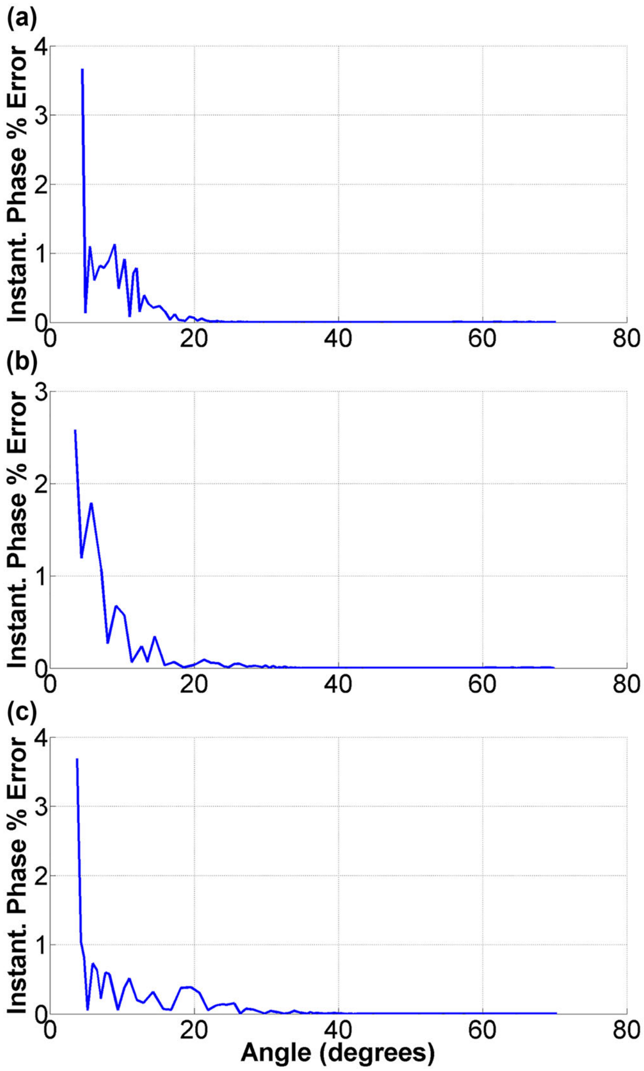

FIGURE 8 Variation of the normalized instantaneous-phase difference {between noise-free and noisy [signal-to-noise ratio (SNR) = 2] data} with the incidence angle for the primary reflection event shown in (a) Figure 6a, (b) Figure 6b and (c) Figure 6c.

TABLE 1 Parameters of the layers in the elastic four-layered model.

Layer	V_P (m/s)	V_S (m/s)	Density (kg/m^3)	Layer thickness (m)
Layer 1	400	100	600	3
Layer 2	520	130	800	8
Layer 3	1500	250	1300	13
Layer 4	1980	330	1500	140

Source: Inspired by field data of Gibbs et al. (1992).

For estimating the uncertainties, we calculate the standard deviation of the relative error between the exact and the estimated phase shifts of each reflection event (Table 2). The error increases noticeably with noise, but it is still acceptable.

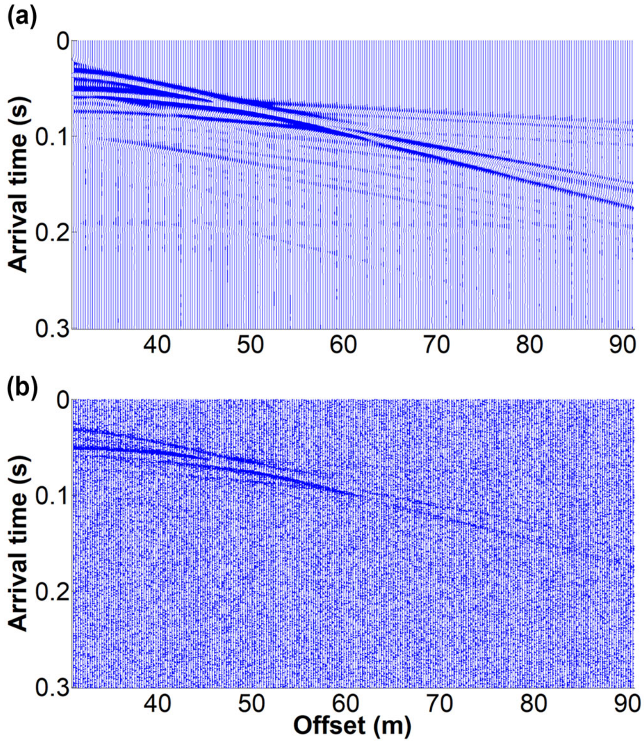

FIGURE 9 Simulated common-source gather using a pressure source on a four-layered elastic model, showing both P- and S-wave reflection events in the case (a) without noise and (b) with noise (signal-to-noise ratio [SNR] = 2) as recorded on the vertical component of a particle-velocity sensor.

For all tested synthetic models, obtaining the exact incidence angle or the trace closest to the CA is difficult, as the region of a phase shift of around 180° is broad. However, the approach is quite successful in finding the correct phase shift/rotation itself and subsequently to correct for it.

In this experiment, we have considered a relatively complex scenario where multiple reflections interfere with each other and random noise with a different wavelet type is added. These conditions allow us to understand how the approach can deal with these challenges. As this approach is based on a given mathematical definition for a wavelet, it is capable of discriminating different kinds of wavelets by a phase analysis and by observing the difference in curve-fitting in each trace. This is possible because the phases would not match if the observed wavelet is of different type than the mathematical description used for the calculated wavelet (e.g., a Gaussian as the observed wavelet and a Ricker wavelet as the calculated one). For this reason, it would result in higher error, which can be an indicator that the wavelets are different. Different from this scenario, interfering reflections with similar amplitudes would generally cause a decrease of the SNR. However, as the approach is able to decompose

 Near Surface Geophysics EAGE EUROPEAN ASSOCIATION OF GEOSCIENTISTS & ENGINEERS

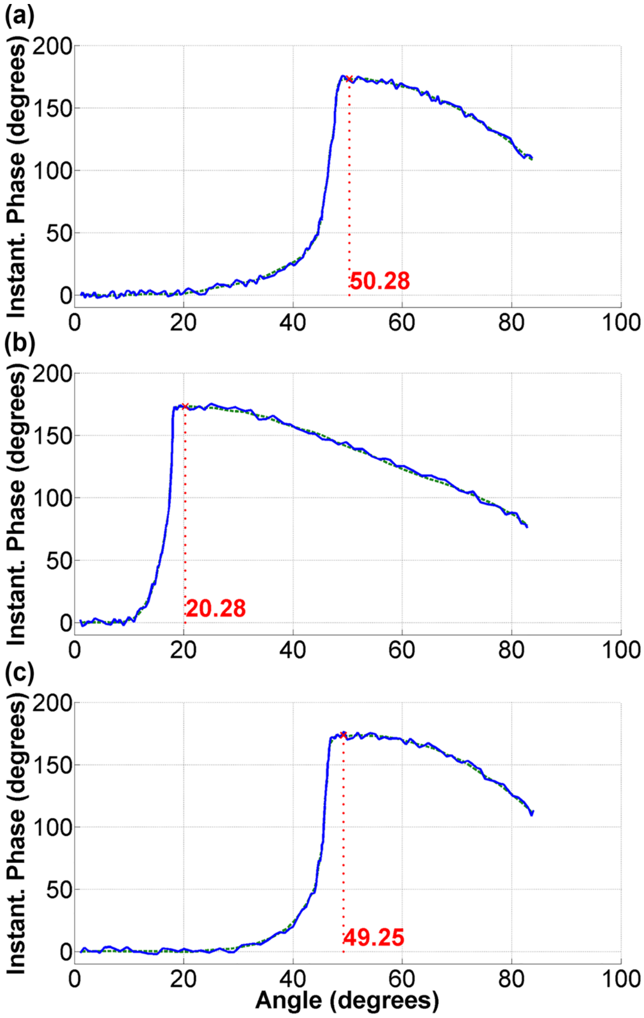

FIGURE 10 Variation of the instantaneous phase with the incident angle for data without noise (dashed green line) and with noise having signal-to-noise ratio (SNR) = 2 (bold blue line), for the PP reflection event in (a) the first layer, (b) the second layer and (c) the third layer. The exact critical angle (CA) is indicated in red, for comparison.

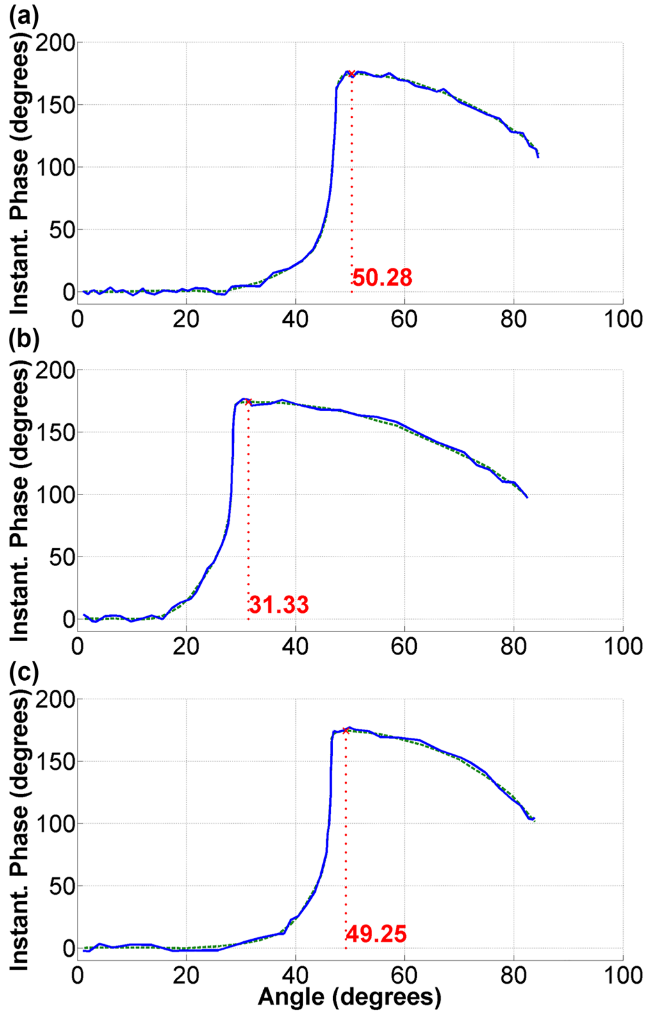

FIGURE 11 Same as in Figure 10, but for the SS reflection event.

the signals, the separation of the wavelets is possible, which will effectively increase the SNR.

Field-data application

We test our approach on the reflection events from a field dataset. These data were recorded near Rotterdam, the Netherlands (Ghose & Goudswaard, 2004). The data were recorded along a 2D line with an S-wave source and horizontal-component receivers oriented in the cross-line direction. The data were processed to suppress the surface waves and the free-surface multiples (Ghose & Goudswaard, 2004). Figure 13a shows a common-source gather, whereas Figure 13b illustrates a CMP gather. We use both these gathers to estimate the instantaneous-phase variation corresponding to the earliest four reflection events.

Despite surface waves and multiple suppressions, a successful application of the proposed approach on field data appears relatively more challenging. In Figure 14, we show the variation of the instantaneous phase with trace offset for the common-source gather and for the CMP gather. For the first reflection event in Figure 13, Figure 14a,e shows a quick increase in the phase shift. For the second reflection event (Figure 14b,f), we do not observe any significant phase shift, indicating that there is no CA possibly due to the underlying layer having a lower S-wave velocity than the upper layer. For the third event, in Figure 14c, we observe a gentle increase, whereas in Figure 14g, no increase can be traced. This might be indicating a larger CA which cannot be seen with limited number of traces available for this interface. For Figure 14d,h, a gentler increase in phase shift can be observed. These results suggest that our approach is

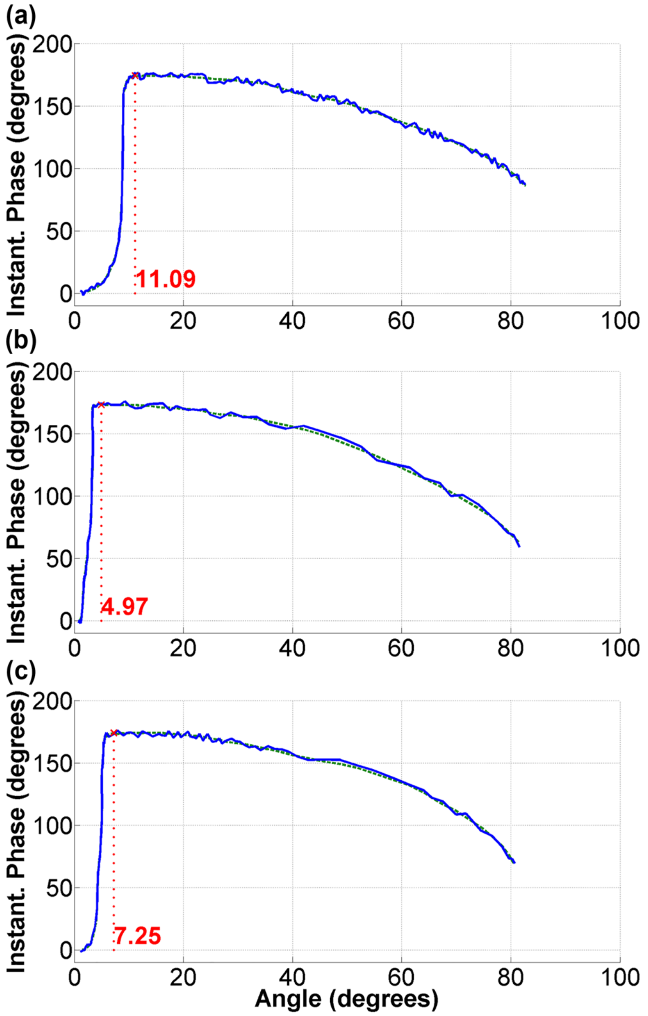

FIGURE 12 Same as in Figure 10, but for the SP reflection event.

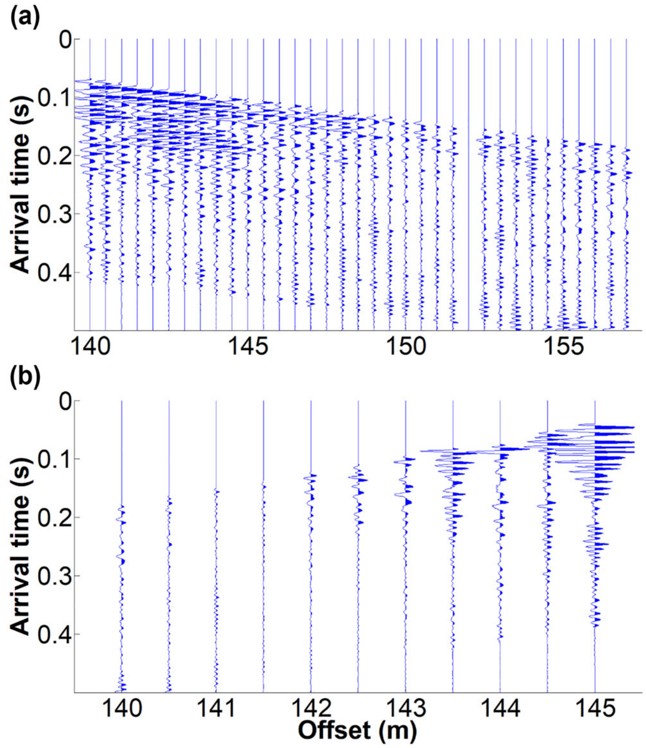

FIGURE 13 Field S-wave reflection data after surface-wave and free-surface multiple suppressions: (a) common-source gather and (b) common-mid-point gather.

successful in finding the correct phase shift/rotation for subsequent use to correct for this shift.

We examined the extent that the reflection amplitude in the stacked section is improved when the phase-corrected traces are used in stacking. In Figure 15, we illustrate the stacked trace (repeated four times for easier visualization) with (Figure 15a) and without (Figure 15b) compensating for the phase rotation using our approach. Clearly, with our approach, the four events are better stacked, exhibiting higher amplitudes and better SNR.

CONCLUSIONS

We proposed an approach for estimating the phase shift of each wavelet representing a reflection event by reconstructing the seismic spectrum through an inversion based on spectral recomposition. We applied this method by calculating the spectrum that best-fits an observed spectrum, and then estimating the instantaneous phase that best-fits the observed instantaneous phase. The proposed method does not require any prior velocity and/or critical-angle information.

TABLE 2 Standard deviation of the relative errors of the phase-shift estimates of the PP, SS and SP reflection events from each of the three interfaces for noise-free and noisy (signal-to-noise ratio [SNR] = 2) data.

Reflection event from interface	PP (noise-free) (%)	PP (noisy) (%)	SS (noise-free) (%)	SS (noisy) (%)	SP (noise-free) (%)	SP (noisy) (%)
1	0.08	1.49	0.06	0.98	0.10	1.78
2	0.08	2.23	0.07	1.67	0.12	2.39
3	0.09	4.63	0.07	3.51	0.13	5.17

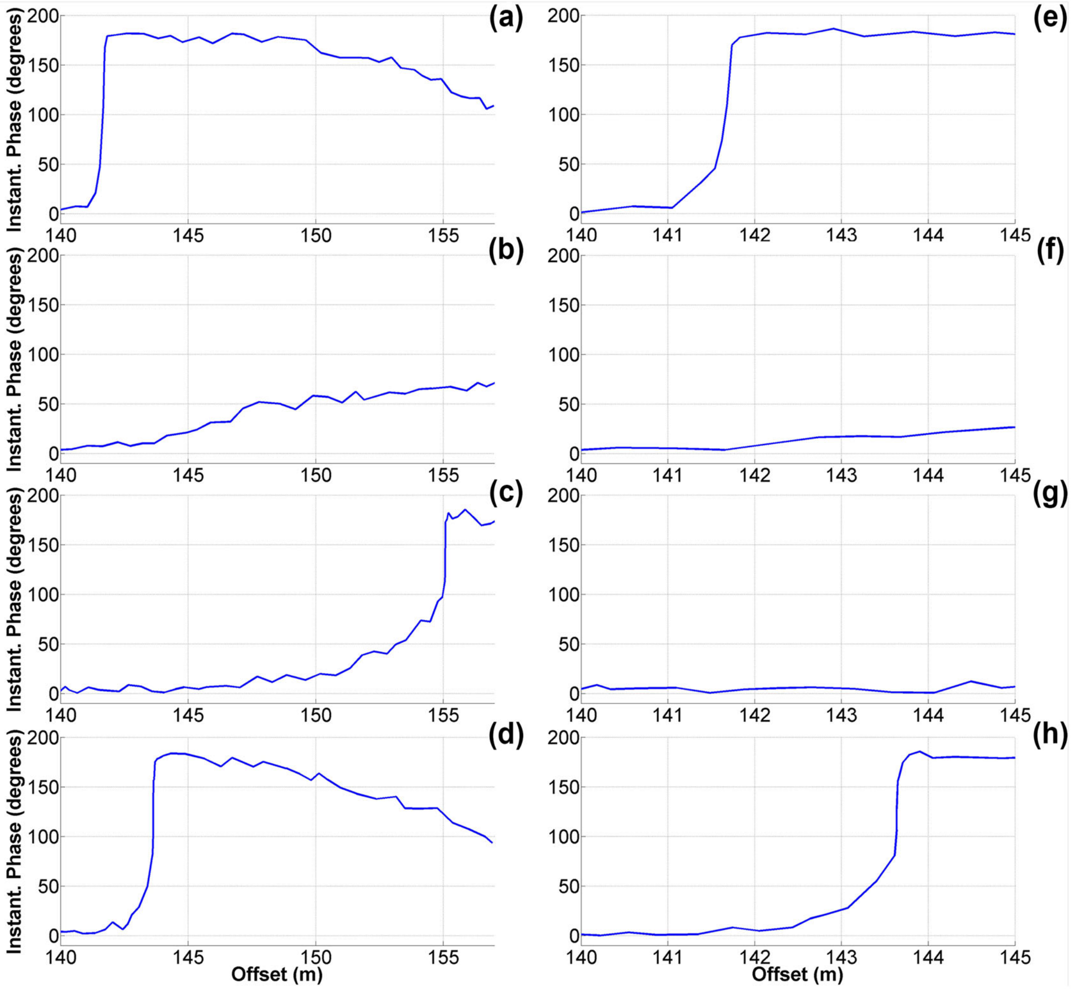

FIGURE 14 Variation of the instantaneous phase with the offset in the field common-source gather for (a) the first, (b) the second, (c) the third and (d) the fourth reflection event. Variation of the instantaneous phase with the offset in the common-mid-point (CMP) gather for (e) the first, (f) the second, (g) the third and (h) the fourth reflection event.

In order to examine the phase-shift estimation for different CAs, we tested our approach on numerically modelled data representing S-wave reflections for three two-layered near-surface models. We also tested our approach using synthetic elastic wavefield data corresponding to a four-layered model. This model is inspired by a field seismic dataset from a site where the water table is located at 13 m depth. Common-source gathers containing both P- and S-wave reflections without and with noise were synthesized. We estimated the phase shift for the reflection wavelet corresponding to PP, SS and PS reflection events. First, we calculate the frequency spectrum and then the instantaneous phase. We showed that it is possible to estimate the phase shift of the near-surface elastic reflection events in a data-driven manner without performing velocity analysis and/or a priori CA estimation, even when there is significant noise in the data. Finally, we tested our approach on field data representing near-surface SH-wave reflections. We showed that with the correction for the phase rotation, as achieved through our approach, the stacked reflection events exhibit higher amplitudes compared to stacking without such corrections. The method that we proposed here offers a new means to estimate correctly the phase shift of the reflection event beyond the CA. This, in turn, allows the correction of the phase shift as a function of the incidence angle in a data-driven manner.

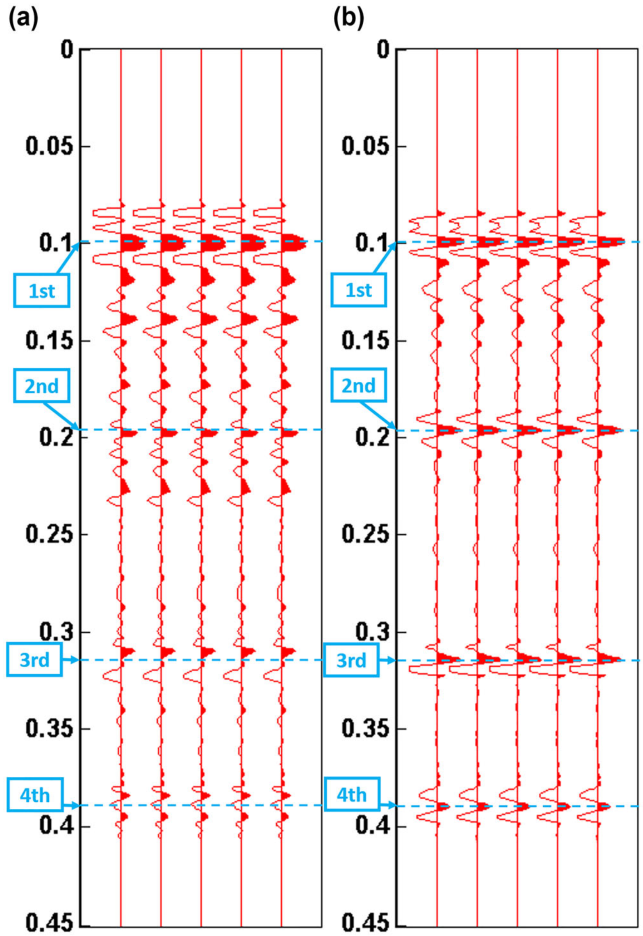

FIGURE 15 Stacked common-mid-point (CMP) sections from near-surface seismic field data: (a) without and (b) with correction for the phase rotation using the proposed approach. The reflection events are marked by the blue dashed lines.

ACKNOWLEDGEMENTS

This study was financed in part by the Coordenação de Aperfeiçoamento de Pessoal de Nível Superior – Brasil (CAPES) – Finance Code 001 and by the Conselho Nacional de Desenvolvimento Científico e Tecnológico – Brasil (CNPq).

DATA AVAILABILITY STATEMENT

In the manuscript, we give the parameters to generate the models and the software we used.

ORCID

Nelson Ricardo Coelho Flores Zuniga https://orcid.org/0000-0002-3633-5721

REFERENCES

Balestrini, F., Draganov, D., Malehmir, A., Marsden, P. & Ghose, R. (2020) Improved target illumination at Ludvika mines of Sweden through seismic-interferometric noise reduction. *Geophysical Prospecting*, 68, 200–213.

Barros, T., Covre, M., Takahata, A.K. & Lopes, R. (2015) Normal moveout with phase equalization. In: *14th International Congress o the Brazilian Geophysical Society*. Brazilian Geophysical Society. pp. 1306–1311. Rio de Janeiro: Brazilian Geophysical Society.

Biondi, E., Stucchi, E. & Mazzoti, A. (2014) Nonstretch normal moveout through iterative partial correction and deconvolution. *Geophysics*, 79(4), V131–V141.

Cai, Y., Fomel, S. & Zeng, H. (2013) Automated spectral recomposition with application in stratigraphic interpretation. *Interpretation*, 1(1), 109–116.

Castagna, J.P., Sun, S. & Siegfried, R.W. (2003) Instantaneous spectral analysis: detection of low-frequency shadows associated with hydrocarbons. *The Leading Edge*, 22, 120–127.

Ghose, R. & Goudswaard, J. (2004) Integrating S-wave seismic-reflection data and cone penetration test data using a multiangle multiscale approach. *Geophysics*, 69, 440–459.

Gibbs, J.F., Fumal, T.E., Boore, D.M. & Joyner, W.B. (1992) Seismic velocities and geologic logs from borehole measurements at seven strong-motion stations that recorded the 1989 Loma Prieta earthquake. *U.S. Geological Survey Open-file Report 92-287*. Menlo Park, California.

Huang, N.E., Shen, Z., Long, S.R., Wu, M.C., Shih, H.H., Zheng, Q. et al. (1998) The empirical mode decomposition and the Hilbert spectrum for nonlinear and non-stationary time series analysis. *Proceedings: Mathematical, Physical and Engineering Sciences*, 454(1971), 903–995.

Landro, M., & Tsvankin, I. (2006) Seismic critical-angle reflectometry: a method to characterize azimuthal anisotropy? In: *SEG New Orleans Annual Meeting*. pp. 120–124. Society of Exploration Geophysicists.

Li, Y., Zheng, X. & Zhang, Y. (2011) High-frequency anomalies in carbonate reservoir characterization using spectral decomposition. *Geophysics*, 76, V47–V57.

Liu, G., Fomel, S. & Chen, X. (2011) Time-frequency analysis of seismic data using local attributes. *Geophysics*, 76(6), P23–P34.

Paskvich, S.W. (2016) Phase-shift measurement analyses of time-lapse multicomponent seismic data over a multi-well hydraulic stimulation, Wattenberg field, Denver basin [Master's Dissertation]. pp. 53. Colorado: Colorado School of Mines.

Purves, S. (2014) Phase and the Hilbert transform. *The Leading Edge*, 33(10), 1164–1166.

Ricker, N. (1953) The form and laws off propagation of seismic wavelets. *Geophysics*, 18, 10–40.

Roth, M., Holliger, K. & Green, A.G. (1998) Guided waves in near-surface seismic surveys. *Geophysical Research Letters*, 25(7), 1071–1074.

Telraky, T. & Sotirov, R. (2013) Multi-start approach for an integer determinant maximization problem. *Optimization*, 61, 101–114.

Thorbecke, J. & Draganov, D. (2011) Finite-difference modeling experiments for seismic interferometry. *Geophysics*, 76, H1–H18.

Tomasso, M., Bouroullec, R. & Pyles, D.R. (2010) The use of spectral recomposition in tailored forward seismic modeling of outcrop analogs. *AAPG Bulletin*, 94(4), 457–474.

Zelt, C.A., Haines, S., Powers, M.H., Sheehan, J., Rohdewald, S., Link, C. et al. (2013) Blind test of methods for obtaining 2-D near-surface seismic velocity models from first-arrival traveltimes. *Journal of Environmental and Engineering Geophysics*, 18(3), 157–197.

Zhu, X. & McMechan, G. (2012) Analysis of phase variation with ray parameter in the τ-p domain. In: *SEG Las Vegas Annual Meeting*. pp. 1–5. Las Vegas: Society of Exploration Geophysicists.

Zuniga, N.R.C.F., Gioria, R.S. & Carmo, B.S. (2023) Spectral recomposition for initial velocity models in full-waveform inversion. *Journal of Applied Geophysics*, 215, 105120.

Zuniga, N.R.C.F., Draganov, D. & Ghose, R. (2023) Critical angle of reflections and Poisson's ratio from spectral recomposition. *Journal of Applied Geophysics*, 215, 105110.

How to cite this article: Zuniga, N.R.C.F., Draganov, D. & Ghose, R. (2023) Phase-shift correction of seismic reflections by means of spectral recomposition. *Near Surface Geophysics*, 1–13. https://doi.org/10.1002/nsg.12271